

This discussion paper is/has been under review for the journal Atmospheric Measurement Techniques (AMT). Please refer to the corresponding final paper in AMT if available.

# Correction of static pressure on a research aircraft in accelerated flight using differential pressure measurements

**A. R. Rodi and D. C. Leon**

Department of Atmospheric Science, University of Wyoming, Laramie, Wyoming, USA

Received: 9 April 2012 – Accepted: 28 April 2012 – Published: 21 May 2012

Correspondence to: A. R. Rodi (rodi@uwyo.edu)

Published by Copernicus Publications on behalf of the European Geosciences Union.

## Correction of static pressure on a research aircraft in accelerated flight

A. R. Rodi and D. C. Leon

Title Page

Abstract

Introduction

Conclusions

References

Tables

Figures

⏪

⏩

◀

▶

Back

Close

Full Screen / Esc

Printer-friendly Version

Interactive Discussion

## Abstract

Geometric altitude data from a combined Global Navigation Satellite System (GNSS) and inertial measurement unit (IMU) system on the University of Wyoming King Air research aircraft are used to estimate acceleration effects on static pressure measurement. Using data collected during periods of accelerated flight, comparison of measured pressure with that derived from GNSS/IMU geometric altitude show that errors exceeding 150 Pa can occur which is significant in airspeed and atmospheric air motion determination. A method is developed to predict static pressure errors from analysis of differential pressure measurements from a Rosemount model 858 differential pressure air velocity probe. The method was evaluated with a carefully designed probe towed on connecting tubing behind the aircraft – a “trailing cone” – in steady flight, and shown to have a precision of about  $\pm 10$  Pa over a wide range of conditions including various altitudes, power settings, and gear and flap extensions. Under accelerated flight conditions, compared to the GNSS/IMU data, this algorithm predicts corrections to a precision of better than  $\pm 20$  Pa. Some limiting factors affecting the precision of static pressure measurement on a research aircraft are examined.

## 1 Introduction

Static pressure measurement on an aircraft is inherently problematic because the pressure changes as the air accelerates around the wings and fuselage as predicted by the Bernoulli equation. It is difficult to find a location on the aircraft to measure the true undisturbed pressure,  $P_\infty$ , i.e., the pressure at a distance far from flow-disturbing effects. On the aircraft, static pressure  $P_s$  is measured at a set of ports where the aircraft designers have determined that the error, referred to as the *static defect* or *position error*, is minimal (Brown, 1988). In addition to causing errors in pressure-derived aircraft altitude, the static defect also leads directly to errors in airspeed and other measurements which need dynamic corrections such as temperature, for example. In

## Correction of static pressure on a research aircraft in accelerated flight

A. R. Rodi and D. C. Leon

Title Page

Abstract

Introduction

Conclusions

References

Tables

Figures



Back

Close

Full Screen / Esc

Printer-friendly Version

Interactive Discussion





flown legs. More recently, Parish et al. (2007) and Parish and Leon (2012) demonstrated that Global Navigation Satellite System (GNSS, hereafter referred to as global positioning system – GPS) data can resolve both pressure gradients and perturbations associated with mesoscale and cloud-scale systems.

In this study, we develop and test a method for estimating static defect using differential pressure measurements. We verify the method using a trailing sonde designed for pressure calibration, and then we compare the method with accurate altitude measurements from a GPS-aided inertial measurement unit (IMU) to examine effects of aircraft acceleration.

## 2 Retrieval of static pressure error from differential pressure measurements

Crawford and Dobosy (1992) describe the Best Aircraft Turbulence (BAT) differential pressure flow-angle probe which addresses the static pressure problem by averaging pressure on several ports. Here, we develop a method to predict the static pressure error directly by using pressure measurements from the Rosemount model 858 (R858) gust probe which on the UWKA is mounted at the tip of a boom as shown in Fig. 1. The probe is a hemisphere-cylinder configuration in which a hemispherical surface is at the end of a 2.5 cm diameter, 12.5 cm long, cylindrical section. Pressure measurements on ports in hemispherical surface are used to for airspeed and flow angle determination (Brown et al., 1983). There are 5 ports: one central port which approximates total pressure, two ports separated by  $\pm 45^\circ$  from the central axis in the aircraft horizontal plane for sideslip angle determination, and two ports separated by  $\pm 45^\circ$  in the aircraft vertical plane for attack angle determination.

In the UWKA system, four differential pressure measurements are made, over-constraining the solution as will be shown, allowing the static error to be estimated. The method and specific equations used in the UWKA R858 configuration are presented in Appendix A. The pressure ports on the R858 are drilled at  $\theta = 45^\circ$  from the

### Correction of static pressure on a research aircraft in accelerated flight

A. R. Rodi and D. C. Leon

Title Page

Abstract

Introduction

Conclusions

References

Tables

Figures



Back

Close

Full Screen / Esc

Printer-friendly Version

Interactive Discussion



central axis, and the attack angle  $\alpha$ , for example, can be estimated as described in the manufacturer's technical note (Rosemount, 1976) with

$$\alpha \simeq \frac{P_{\alpha 1} - P_{\alpha 2}}{K q_c} \quad (1)$$

where the numerator is the differential pressure between the two attack angle ports. The sensitivity coefficient, assuming potential flow ( $f = 9/4$ ) for small angles, is  $K \cong 2f(\pi/180) = 0.0785 \text{ deg}^{-1}$ . Brown et al. (1983) investigated  $K$  using data from flight maneuvers for the R858 on the noseboom on the NCAR Sabreliner. They found that for  $N_{\text{Mach}} < 0.5$ ,  $K = 0.068 \text{ deg}^{-1}$  ( $f = 1.95$ ), 13% lower than the value recommended in (Rosemount, 1976). This determination of  $K$  was not exact nor without ambiguities, however. The Brown et al. (1983) method substituted precise IMU-measured pitch angle for attack angle which is valid during periods of straight and level flight assuming zero vertical wind and aircraft vertical velocity, implicitly assuming the upwash effect was negligible. The sense of upwash effect is to make the local attack angle larger than the pitch angle. This underestimation of local attack angle would then cause  $K$  to be overestimated. Brown et al. (1983) suggest that the reason this could be possibly the effect of not accounting for flow distortion (upwash) effects, or errors in total and static pressure. However, correcting for these effects would reduce the  $K$  estimates from the manufacturer's value.

We will show that the static pressure error can be determined from the differential pressure measurements assuming that sensitivity factor  $f$  can be determined. The unknowns in the four differential pressure Eq. (A11) in the Appendix are the attack angle  $\alpha$ , sideslip angle  $\beta$ ,  $q$ , and  $f$  which are sufficient for an exact solution. If we now allow for the measured static pressure to be in error, then the first equation in the set (A11) becomes

$$\Delta P_1 = P_1 - (P_{s,m} - P_{\text{err}}) = q \left[ 1 - \frac{f(\tan^2 \alpha + \tan^2 \beta)}{1 + \tan^2 \alpha + \tan^2 \beta} \right] \quad (2)$$

**Correction of static pressure on a research aircraft in accelerated flight**

A. R. Rodi and D. C. Leon

Title Page

Abstract

Introduction

Conclusions

References

Tables

Figures

◀

▶

◀

▶

Back

Close

Full Screen / Esc

Printer-friendly Version

Interactive Discussion



where  $P_{s,m}$  is the measured pressure, and  $P_{err}$  is the error correction, now an additional unknown. If the sensitivity factor  $f$  is known, then  $P_{err}$  can be estimated as the unknown quantity.

### 3 Trailing cone test data

Ikhtiari and Marth (1964) and Mabry and Brumby (1968) describe a aircraft pressure calibration system in which a static pressure probe, connected to the aircraft by tubing, is towed at some distance behind and below the aircraft, away from the disturbing influence of the aircraft. The towed sonde is stabilized in flight by means of a carefully engineered cone – thus the term “trailing cone” (hereafter called TC) – that creates drag for stabilization of static pressure ports which are distributed around the circumference of a straight piece of tubing behind the cone. Brown (1988) described the technique in detail, and demonstrated for the NCAR Sabreliner that the largest expected error in the pressure measurement is  $\pm 39$  Pa after application of corrections based upon the TC data. The distance that the TC is extended is chosen to be long enough to minimize pressure fluctuations in the aircraft’s wake. However, accelerations cause errors. For example, with a 19 m tubing length (the length used for the UWKA), a 0.1 g acceleration will result in a 15 Pa effect. Consequently, we limit data collection to steady, straight flight legs.

A UWKA test flight using the Douglas model 501 TC was conducted on 27 October 2005. Data were collected in several configurations: (1) with the aircraft in “clean” configuration (landing gear raised, flaps retracted), (2) in segments with gear lowered, (3) with gear lowered and flaps extended in approach mode, and (4) at different power settings and altitudes. Several measured variables are shown in Fig. 2 as a function of aircraft attack angle, using data filtered at 5 Hz and output at 10 Hz. The lack of a single relationship for all configurations among dynamic pressure, pressure error, and  $N_{Mach}$  is evident. This is the main obstacle to simple corrections as a function of one variable such as dynamic pressure or attack angle.

## Correction of static pressure on a research aircraft in accelerated flight

A. R. Rodi and D. C. Leon

Title Page

Abstract

Introduction

Conclusions

References

Tables

Figures

◀

▶

◀

▶

Back

Close

Full Screen / Esc

Printer-friendly Version

Interactive Discussion



## 4 Empirical determination of $f$ from trailing cone data

We solved Eqs. (2) and (A11) using TC flight measurements of  $P_{err}$  to directly obtain the unknown values of  $f$ . These are plotted in Fig. 3, and show an increase in  $f$  with  $\Delta P_\alpha$ , and decrease with  $N_{Mach}$ . We then used a non-linear regression procedure to obtain the empirical estimate of  $f$  which best predicts the TC  $P_{err}$ . The best fit was found by trial and error to be:

$$f = c_0 + c_1 N_{Mach} + c_2 N_{Mach}^2 + c_3 \Delta P_\alpha \quad (3)$$

where the constants were found to be  $c_0 = 1.700$ ,  $c_1 = -0.1569$ ,  $c_2 = 0.06633$ , and  $c_3 = +0.001254$ , where  $\Delta P_\alpha$  is in units of hPa. A discussion of the physical basis for these relationships will be presented later.

The resulting predictions of pressure error are compared with TC measurements in Fig. 4 at various steady flight configurations and power settings with the TC measurements. The distribution of the residual errors is shown in Fig. 5 to be  $\pm 20$  Pa in all configurations ( $\sigma = 8$  Pa).

There is additional evidence for the variability of  $f$ . Brown et al. (1983) and Rosemount (1976) provide experimental evidence for  $f$  decreasing with  $N_{Mach}$ , consistent with the present results. Traub and Rediniotis (2003) (TR03) present an analytical prediction of surface pressures for a hemisphere-cylinder configuration similar to the R858, and wind tunnel results at Reynolds numbers about a factor of two higher than UWKA flight ( $N_{Re} \approx 1.5 \cdot 10^4$ ). The TR03 theoretical formulation, confirmed by their wind tunnel results, predicts sensitivity to be  $f = 2.07$  at zero incidence angle, and also their data shows that the sensitivity varies with incidence angle.

To explore the effect of probe shape on  $f$ , we used a commercially-available finite-element solver for turbulent, compressible flow equations (FIDAP, Fluid Dynamics International, Inc.) An axisymmetric, compressible model at zero attack angle was used and showed that  $f$  is different for various mounting configurations, and changes with speed. Solutions were found for  $N_{Mach}$  equivalent to speeds of 50–180  $\text{m s}^{-1}$ . Four configurations were modeled as show in Fig. 6 (not to scale): (1) a sphere (not shown); (2)

### Correction of static pressure on a research aircraft in accelerated flight

A. R. Rodi and D. C. Leon

Title Page

Abstract

Introduction

Conclusions

References

Tables

Figures

⏪

⏩

◀

▶

Back

Close

Full Screen / Esc

Printer-friendly Version

Interactive Discussion



## Correction of static pressure on a research aircraft in accelerated flight

A. R. Rodi and D. C. Leon

Title Page

Abstract

Introduction

Conclusions

References

Tables

Figures

⏪

⏩

◀

▶

Back

Close

Full Screen / Esc

Printer-friendly Version

Interactive Discussion

the R858 probe mounted on the end of the UWKA nose boom which is 0.2 m in diameter; (3) the spherical radome (nose radar covering) as on the former National Science Foundation (NSF) King Air aircraft (N308D); and (4) the R858 mounted on a nose boom four times the diameter of the actual UWKA nose boom. Pressure distributions on the spherical surface were fit using the  $\sin^2$  relationship and the resulting  $f$  for each  $N_{\text{Mach}}$  plotted in Fig. 7a. For the sphere,  $f$  varies from 1.9–2.1. As in the wind tunnel model, adding the nose boom behind the R858 hemisphere-cylinder decreases  $f$  to about 1.9. Increasing the boom diameter to 0.8 m lowers  $f$  to about 1.5. These results suggest that there is no unique value of  $f$  for all mounting configurations of the R858. Indeed, the fuselage of the aircraft itself presents a formidable aerodynamic barrier to the probe which is likely to contribute to the actual  $f$  variability in addition to a particular mounting configuration.

To explore further the behavior of  $f$ , we constructed a physical model of the R858 with extra pressure ports drilled so that adequacy of the  $\sin^2$  relationship between angle and pressure could be determined by direct measurement along with determination of  $f$ . The test was conducted in the University of Wyoming Low Speed Wind Tunnel, which has a test section of  $0.6 \times 0.6 \times 0.9$  m. The model was constructed 75 % larger than the actual probe so that the Reynolds number at the test speed of  $50 \text{ ms}^{-1}$  would be approximately that of the actual (0.0254 m diameter) probe at  $90 \text{ ms}^{-1}$ , the typical flight speed for the UWKA. Data were digitized with a personal-computer-based data logging system at 10 Hz after analog filtering with cutoff frequency of 2 Hz. The analysis then was performed on one minute averages of pressures at each port. Additional measurements made with a standard pitot tube placed upwind from the test body to ensure that the tunnel speed did not change during runs at each attack angle. In Fig. 7b, the sensitivity of  $f$  to  $N_{\text{mach}}$  from Brown et al. (1983) and (Rosemount, 1976) is shown, along with  $f$  determined from the wind tunnel tests (point labeled as “T”), and the solution of Eq. (A11) with actual King Air flight data.

## 5 Measured pressure compared pressure derived from GPS altitude

While the 2005 TC test flight varied attack angle with airspeed and altitude, sideslip angles were intentionally kept near zero to prevent lateral acceleration. In this section, the efficacy of the estimates of  $P_{err}$  in an accelerating flight environment using the differential pressure (hereafter DP) solution described in the previous section will be examined.

Differential global positioning system (dGPS) techniques use data from one or more stationary reference or base GPS stations which have precisely determined location to refine position estimates for the receiver on the aircraft. dGPS processing techniques using dual-frequency (L1/L2) carrier phase data can eliminate errors caused by ionospheric and tropospheric delays entirely, resulting in position estimates with accuracy of centimeters under optimal conditions (Parish et al., 2007).

In the present study, we use post-processed inertial measurement unit (IMU) data in conjunction with dual-frequency dGPS data to resolve the aircraft position and motion (Trimble/Applanix model AV410). The IMU data, recorded at 200 Hz, were corrected in post-processing using Trimble/Applanix POSPac software which implements a tightly-coupled Kalman filter between the IMU and dGPS data. The processing fully removed all L1/L2 cycle ambiguities in a fixed, narrow lane processing mode. Position accuracy estimated by the manufacturer is shown in Table 1. The resulting 200 Hz values of aircraft position and attitude were low-pass filtered with a cutoff frequency of 10 Hz and then decimated to 20 Hz for the present analysis. Also, accurate time synchronization of the IMU and pressure measurements was assured by GPS time stamping of all data.

Static pressure was measured with the Rosemount 1501 High Accuracy Digital Sensing Module (HADS) which has static accuracy of 20 Pa and a digital resolution of 1.8 Pa. The accuracy includes effects of non-linearity, repeatability, temperature ( $-51$  to  $80^{\circ}\text{C}$ ) and calibration. Worst case error from transducer acceleration is specified to be 20 Pa under acceleration of 6 g – the maximum acceleration in these tests was  $\pm 1$  g. We estimate the maximum dynamic errors in the connecting tubing to be 10 Pa

## Correction of static pressure on a research aircraft in accelerated flight

A. R. Rodi and D. C. Leon

Title Page

Abstract

Introduction

Conclusions

References

Tables

Figures

⏪

⏩

◀

▶

Back

Close

Full Screen / Esc

Printer-friendly Version

Interactive Discussion



for longitudinal accelerations (here 0.1 g, 10 m tubing length) and lateral (1 g, 1 m tubing length) accelerations of the air column.

Flight data were collected on 16 September 2011 during pilot-induced maneuvers inducing variations in attack and sideslip angles. Periods of turns not considered in the analysis. The aircraft was flown at nominally constant pressure with deviations corrected hydrostatically to that pressure using the method described by Parish et al. (2007). Pressure-derived altitude changes were determined from integration of the hydrostatic equation:

$$z - z_0 = - \int_{P_0}^P \frac{R_{\text{dry}} T_v}{g} d \ln P \quad (4)$$

where  $z_0$  is a direct measurement of geometric altitude from the IMU/dGS system at pressure  $P_0$  and virtual temperature  $T_v$ . Data were collected at two altitudes – nominally 4600 and 7000 m m.s.l. Other relevant measurements include: in-house developed reverse flow temperature (accuracy of 0.5 K, resolution of 0.006 K), and Edgetech Model 137 dew point temperature (accuracy of 1 K, resolution 0.006 K).

A bias is introduced if an atmospheric horizontal pressure gradient exists, or when pressure is falling, along the flight track since constant geometric height is no longer constant pressure. To minimize this effect, the time series is broken up into 500 s segments and reinitialized with  $z_0$  from the highly accurate IMU/dGPS geometric altitude value at that instant. The Laramie Valley was under the influence of high pressure, clear sky, and weak pressure gradient during the analysis period which minimized the pressure change effect.

Computing geometric altitude from measured static pressure also involved careful consideration the relative distance vectors of the inertial measurement unit (IMU), GPS antenna, R858, and the static pressure locations. These vectors were accurately determined with accuracy <5 cm using precise surveying techniques. The “lever arm”

**Correction of static pressure on a research aircraft in accelerated flight**

A. R. Rodi and D. C. Leon

Title Page

Abstract

Introduction

Conclusions

References

Tables

Figures



Back

Close

Full Screen / Esc

Printer-friendly Version

Interactive Discussion





whitening effect of the digitization noise (2 Pa). The sharp disturbances at 30–40 Hz in Fig. 14 (sideslip periods) are probably due to the 4-bladed propellers which operate normally at about 1700 rpm.

## 7 Conclusions

5 An algorithm was developed to estimate static pressure errors in steady flight using R858 differential pressure measurements, and tested with trailing cone data from a University of Wyoming King Air flight in 2005. Using the R858 measurements to estimate static pressure error, it was shown that the effects speed, altitude and flight configuration (landing gear, flap extension) can be predicted to  $\sigma = 8$  Pa in steady flight. To  
10 capture the effects of acceleration, flight maneuvers were conducted, and geometric altitude measured with a GPS-aided inertial measurement data was used to predict the pressure error. These results suggest that pressure errors can be determined with a precision of  $\pm 20$  Pa during such maneuvers. It should be emphasized that the precision, not the absolute accuracy of these estimates, is addressed in this paper. The  
15 absolute accuracy of the error estimates using this method depend on this empirical determination of  $f$  as well as other factors addressed in the present work.

Our attempts to use statistical regression analysis alone to relate the observed pressure error to flight data ( $N_{Mach}$ ,  $q_c$ , inertial acceleration) have not been successful. The differential pressure method, however, has the advantage of being a solution based  
20 upon the R858 equations as presented in the Appendix. The main weakness is that the probe sensitivity  $f$  requires an independent means of its determination. In the present study, we used the TC measurements to calibrate  $f$ .

There are several sources of error which may be a factor in the interpretation. The effect of acceleration of the air in the connecting tubing, which we estimate to be smaller  
25 than 10 Pa, is indistinguishable from the aerodynamic cause of the static defect at the sensing ports. Nonetheless, the R858 pressure imbalance approach would capture the connecting tubing effect. The other factor is the error introduced by uncertainty in height

### Correction of static pressure on a research aircraft in accelerated flight

A. R. Rodi and D. C. Leon

Title Page

Abstract

Introduction

Conclusions

References

Tables

Figures

◀

▶

◀

▶

Back

Close

Full Screen / Esc

Printer-friendly Version

Interactive Discussion



differences between the static pressure ports at the rear of the fuselage, IMU and GPS antenna locations, and R858 probe tip. Figure 8d shows this effect is <10 Pa.

We speculate that addition of a fifth differential pressure measurement to the R858 would eliminate  $f$  as an unknown. We are currently studying the choices for a fifth pressure measurement which optimizes the ability to resolve static pressure errors, and planning that modification and evaluation for a future study.

## Appendix A

### Derivation of differential pressure equations for a spherical 5-hole probe

The derivation of the relationships among the pressures on a 5-hole spherical probe surface and the attack and sideslip flow angles follows. Hale and Norrie (1967), Brown et al. (1983), and Nacass (1992) analyzed the differential pressures between ports in terms of the well-known pressure distribution on a sphere in terms of the coefficient of pressure  $C_p$ :

$$C_p = \frac{P - P_\infty}{q} = 1 - f \sin^2 \phi \quad (\text{A1})$$

where  $P$  is the pressure at solid angle  $\phi$  from the stagnation point,  $P_\infty$  is the pressure in the free stream,  $\rho$  is the air density,  $q = 1/2\rho U^2$  is the dynamic pressure,  $U$  the speed, and  $f$  the sensitivity factor.  $f = 9/4$  for potential flow (Lamb, 1932).

A coordinate system is defined by unit vectors as follows:  $\hat{i}$  along the x-axis forward through the center port;  $\hat{j}$  along the y-axis to the right, and  $\hat{k}$  long the z-axis down in aircraft coordinates. The angle  $\phi$  in Eq. (A1) is the “great circle” angle between the stagnation point and point of pressure measurement at one of the five ports (Nacass, 1992). We define two more unit vectors in terms of their direction cosines from the

## Correction of static pressure on a research aircraft in accelerated flight

A. R. Rodi and D. C. Leon

Title Page

Abstract

Introduction

Conclusions

References

Tables

Figures

⏪

⏩

◀

▶

Back

Close

Full Screen / Esc

Printer-friendly Version

Interactive Discussion



probe axes: one,  $\hat{\lambda}_0$ , from the center of the probe hemisphere through the stagnation point, and the other,  $\hat{\lambda}_a$ , through the pressure port of interest. Thus,

$$\begin{aligned}\hat{\lambda}_0 &= \hat{i} \cos \theta_{x0} + \hat{j} \cos \theta_{y0} + \hat{k} \cos \theta_{z0} \\ \hat{\lambda}_a &= \hat{i} \cos \theta_{xa} + \hat{j} \cos \theta_{ya} + \hat{k} \cos \theta_{za}\end{aligned}\quad (A2)$$

and the direction cosines for each vector are constrained by the identity

$$\cos^2 \theta_x + \cos^2 \theta_y + \cos^2 \theta_z = 1. \quad (A3)$$

Angle  $\phi$  then can be found from the definition of the cross product of two vectors

$$\sin \phi = |\hat{\lambda}_a \times \hat{\lambda}_0| / |\hat{\lambda}_a| |\hat{\lambda}_0| \quad (A4)$$

which can be expanded as

$$\begin{aligned}\sin^2 \phi &= \cos^2 \theta_{xa} (1 - \cos^2 \theta_{x0}) + \cos^2 \theta_{ya} (1 - \cos^2 \theta_{y0}) \\ &\quad + \cos^2 \theta_{za} (1 - \cos^2 \theta_{z0}) - 2 \cos \theta_{xa} \cos \theta_{ya} \cos \theta_{x0} \cos \theta_{y0} \\ &\quad - 2 \cos \theta_{xa} \cos \theta_{za} \cos \theta_{x0} \cos \theta_{z0} \\ &\quad - 2 \cos \theta_{ya} \cos \theta_{za} \cos \theta_{y0} \cos \theta_{z0}.\end{aligned}\quad (A5)$$

- 10 The coordinate system is defined with regard to aircraft axes as follows: x-axis forward through the center port 1, y-axis right, and z-axis down. Ports 2 (positive) and 3 are in x-y plane, and ports 4 (positive) and 5 in the x-z plane. The center port then has  $\theta_{xa} = 0^\circ$ ,  $\cos \theta_{xa} = 1$ . The equations for  $\phi$  for each port, then are

$$\begin{aligned}\sin^2 \phi_1 &= 1 - \cos^2 \theta_{x0} \\ \sin^2 \phi_2 &= \cos^2 \theta_{ya} (1 + \cos^2 \theta_{z0} - 2 \cos \theta_{x0} \cos \theta_{y0}) \\ \sin^2 \phi_3 &= \cos^2 \theta_{ya} (1 + \cos^2 \theta_{z0} + 2 \cos \theta_{x0} \cos \theta_{y0}) \\ \sin^2 \phi_4 &= \cos^2 \theta_{za} (1 + \cos^2 \theta_{y0} - 2 \cos \theta_{x0} \cos \theta_{z0}) \\ \sin^2 \phi_5 &= \cos^2 \theta_{za} (1 + \cos^2 \theta_{y0} + 2 \cos \theta_{x0} \cos \theta_{z0}).\end{aligned}\quad (A6)$$

## Correction of static pressure on a research aircraft in accelerated flight

A. R. Rodi and D. C. Leon

Title Page

Abstract

Introduction

Conclusions

References

Tables

Figures

◀

▶

◀

▶

Back

Close

Full Screen / Esc

Printer-friendly Version

Interactive Discussion

## Correction of static pressure on a research aircraft in accelerated flight

A. R. Rodi and D. C. Leon

Title Page

Abstract

Introduction

Conclusions

References

Tables

Figures

◀

▶

◀

▶

Back

Close

Full Screen / Esc

Printer-friendly Version

Interactive Discussion



Four differential pressures are measured:  $P_1 - P_\infty$  which approximately the impact pressure  $q_c$  at small angles,  $P_2 - P_3$  in the plane of the probe horizontal axis defining the sideslip angle  $\beta$ ,  $P_4 - P_5$  in the plane of the probe vertical axis defining the attack angle  $\alpha$ , and  $P_1 - P_2$  which is also a measure of the impact pressure as suggested by Rosemount (1976) for their Model 858 5-hole probe. The center port then has  $\theta_{xa} = 0^\circ$ ,  $\cos \theta_{xa} = 1$ , and the remaining ports are at  $\theta = 45^\circ$ ,  $\cos \theta_{ya} = \cos \theta_{za} = \sqrt{2}/2$ . Combining these angles and differential pressure definitions with Eq. (A6) applied to Eq. (A1) gives the set of equations for the differential pressures:

$$\begin{aligned} P_1 - P_\infty &= q[1 - f(1 - \cos^2 \theta_{x0})] \\ P_2 - P_3 &= 2qf \cos \theta_{x0} \cos \theta_{y0} \\ P_4 - P_5 &= 2qf \cos \theta_{x0} \cos \theta_{z0} \end{aligned} \quad (\text{A7})$$

$$P_1 - P_2 = \frac{1}{2}qf(\cos^2 \theta_{x0} - \cos^2 \theta_{y0} - 2 \cos \theta_{x0} \cos \theta_{y0})$$

We now define the attack angle  $\alpha$  and sideslip angle  $\beta$  as functions of the velocity components in terms of the direction cosines ( $U_x/U = \cos \theta_{x0}$ , etc.):

$$\tan \alpha = \frac{U_z}{U_x} = \frac{U \cos \theta_{z0}}{U \cos \theta_{x0}} = \frac{\cos \theta_{z0}}{\cos \theta_{x0}} \quad (\text{A8})$$

$$\tan \beta = \frac{U_y}{U_x} = \frac{U \cos \theta_{y0}}{U \cos \theta_{x0}} = \frac{\cos \theta_{y0}}{\cos \theta_{x0}}. \quad (\text{A9})$$

Note that  $\beta$  as defined here is not the standard definition of sideslip (ISO, 1985), but is the commonly used definition because of its natural relation to  $U_y$  in the wind computation.

Equations (A8) and (A9) can be solved for the direction cosines as

$$\begin{aligned} \cos \theta_{x0} &= 1/(1 + \tan^2 \alpha + \tan^2 \beta)^{1/2} \\ \cos \theta_{y0} &= \tan \beta / (1 + \tan^2 \alpha + \tan^2 \beta)^{1/2} \\ \cos \theta_{z0} &= \tan \alpha / (1 + \tan^2 \alpha + \tan^2 \beta)^{1/2}. \end{aligned} \quad (\text{A10})$$

Equations (A7)–(A10) can be combined to give the final set of equations:

$$\begin{aligned}\Delta P_1 &= P_1 - P_\infty = q[1 - f(\tan^2 \alpha + \tan^2 \beta)/(1 + \tan^2 \alpha + \tan^2 \beta)] \\ \Delta P_\alpha &= P_4 - P_5 = 2fq \tan \alpha / (1 + \tan^2 \alpha + \tan^2 \beta) \\ \Delta P_\beta &= P_2 - P_3 = 2fq \tan \beta / (1 + \tan^2 \alpha + \tan^2 \beta) \\ \Delta P_R &= P_1 - P_2 = 2fq(1 - 2 \tan \beta - \tan^2 \beta) / (1 + \tan^2 \alpha + \tan^2 \beta).\end{aligned}\tag{A11}$$

Equation (A11) can be solved either numerically or analytically for the unknowns  $\tan \beta$ ,  $\tan \alpha$ ,  $q$  and  $f$ . The  $\Delta P_\alpha$ ,  $\Delta P_\beta$ , and  $\Delta P_R$  equations can be solved analytically  $\tan \beta$ ,  $\tan \alpha$  without a priori knowledge of dynamic pressure  $q$  or sensitivity factor  $f$ . Those solutions are:

$$\begin{aligned}\tan \beta &= (\sqrt{2(\Delta P_\beta^2 + 2\Delta P_\beta \Delta P_R + \Delta P_R^2)} - \Delta P_\beta - 2\Delta P_R) / \Delta P_\beta \\ \tan \alpha &= (\tan \beta) \Delta P_\alpha / \Delta P_\beta.\end{aligned}\tag{A12}$$

We note that the limiting relationship when  $\Delta P_B \rightarrow 0$  is

$$\tan \alpha = \frac{\Delta P_\alpha}{4\Delta P_R}\tag{A13}$$

and

$$q = \frac{\Delta P_\alpha^2 + 8\Delta P_1 \Delta P_R}{8\Delta P_R}.\tag{A14}$$

*Acknowledgements.* The authors would like to thank colleagues in the Department of Atmospheric Science at the University of Wyoming and the UWKA facility team for collection and processing of the data. This study was supported by NSF Cooperative Agreement AGS-0334908, and NSF Grant AGS-1034862.

**Correction of static pressure on a research aircraft in accelerated flight**

A. R. Rodi and D. C. Leon

Title Page

Abstract

Introduction

Conclusions

References

Tables

Figures



Back

Close

Full Screen / Esc

Printer-friendly Version

Interactive Discussion



## References

- Bellamy, J. C.: The use of pressure altitude and altimeter corrections in meteorology, *J. Meteorol.*, 2, 1–79, 1945. 3613
- 5 Brown, E. N.: Position error calibration of a pressure survey aircraft using a trailing cone, Tech. Rep. NCAR/TN-313+STR, National Center for Atmospheric Research, Boulder, CO, 1988. 3612, 3613, 3616
- Brown, E. N., Friehe, C. A., and Lenschow, D. H.: The use of pressure fluctuations on the nose of an aircraft for measuring air motion, *J. Clim. Appl. Meteorol.*, 22, 1070–1075, 1983. 3615, 3618, 3623, 3636
- 10 Brown, E. N., Shapiro, M. A., Kennedy, P. J., and Friehe, C. A.: The application of airborne radar altimetry to the measurement of height and slope of isobaric surfaces, *J. Appl. Meteorol.*, 20, 171–180, 1983. 3613, 3614, 3615, 3617
- Crawford, T. and Dobosy, R.: A sensitive fast-response probe to measure turbulence and heat-flux from any airplane, *Bound.-Lay. Meteorol.*, 59, 257–278, doi:10.1007/BF00119816, 1992. 3614
- 15 Doebelin, E. O.: *Measurement Systems: Application and Design*, McGraw-Hill, New York, 1990. 3613
- Hale, M. R. and Norrie, D. H.: The analysis and calibration the five-hole spherical pitot, Tech. Rep., ASME Publication 67-WA/FE-24, Amer. Soc. Mech. Eng., New York, 1967. 3623
- 20 Ikhtari, P. A. and Marth, V. G.: Trailing cone static pressure measurement device, *J. Aircraft.*, 1, 93–94, 1964. 3616
- ISO: *Flight dynamics, concepts and quantities Part 2: Motions of aircraft and the atmosphere relative to the earth*, 2nd Edn., Ref. No. ISO 1151/2-1985(E), International Organization for Standardization, Geneva, Switzerland, 1985. 3625
- Lamb, H.: *Hydrodynamics*, Dover Publications, New York, 1932. 3623
- LeMone, M. A. and Tarleton, L. F.: The use of inertial altitude in the determination of the convective-scale pressure field over land, *J. Atmos. Ocean. Tech.*, 3, 650–661, 1986. 3613
- LeMone, M. A., Tarleton, L. F., and Barnes, G. M.: Perturbation pressure at the base of cumulus clouds in low shear, *Mon. Weather Rev.*, 116, 2062–2068, 1988. 3613
- 30 Mabry, G. and Brumby, R.: DC-8 Airspeed Static Position Error Repeatability, Tech. Rep., Douglas Paper 5517, Douglas Aircraft Co., Unk., 1968. 3616

### Correction of static pressure on a research aircraft in accelerated flight

A. R. Rodi and D. C. Leon

Title Page

Abstract

Introduction

Conclusions

References

Tables

Figures

⏪

⏩

◀

▶

Back

Close

Full Screen / Esc

Printer-friendly Version

Interactive Discussion



---

**Correction of static pressure on a research aircraft in accelerated flight**

A. R. Rodi and D. C. Leon

---

Title Page

Abstract

Introduction

Conclusions

References

Tables

Figures

⏪

⏩

◀

▶

Back

Close

Full Screen / Esc

Printer-friendly Version

Interactive Discussion



Nacass, P. L.: Theoretical errors on airborne measurements of: static pressure, impact temperature, air flow angle, air flow speed, Tech. Rep., NCAR/TN-385+STR, National Center for Atmospheric Research, Boulder, CO, 1992. 3623

Parish, T. R.: Forcing of the summertime low-level jet along the California coast, J. Appl. Meteorol., 39, 2421–2433, 2000. 3613

5 Parish, T. R. and Leon, D.: Measurement of cloud perturbation pressures using an instrumented aircraft, J. Atmos. Ocean. Tech., accepted, 2012. 3614

Parish, T. R., Rodi, A. R., and Clark, R. D.: A case study of the summertime Great Plains Low Level Jet, Mon. Weather Rev., 116, 94–105, 1988. 3613

10 Parish, T. R., Burkhardt, M. D., and Rodi, A. R.: Determination of the horizontal pressure gradient force using Global Positioning System onboard an instrumented aircraft, J. Atmos. Ocean. Tech., 24, 521–528, 2007. 3614, 3619

Rodi, A. R. and Parish, T. R.: Aircraft measurement of mesoscale pressure gradients and geostrophic winds, J. Atmos. Ocean. Tech., 5, 91–101, 1988. 3613

15 Rosemount: Model 858 flow angle sensors, Tech. Rep., Bulletin 1014, Revised 4/76, Rosemount Engineering, Minneapolis, MN, 1976. 3615, 3617, 3618, 3625, 3636

Shapiro, M. A. and Kennedy, P. J.: Research aircraft measurements of jet stream geostrophic and ageostrophic winds, J. Atmos. Sci., 38, 2642–2652, 1981. 3613

20 Traub, L. and Rediniotis, O.: Analytic prediction of surface pressures over a hemisphere-cylinder at incidence, J. Aircraft, 40, 645–652, doi:10.2514/2.3168, 2003. 3617

## Correction of static pressure on a research aircraft in accelerated flight

A. R. Rodi and D. C. Leon

Title Page

Abstract

Introduction

Conclusions

References

Tables

Figures

⏪

⏩

◀

▶

Back

Close

Full Screen / Esc

Printer-friendly Version

Interactive Discussion

**Table 1.** Trimble/Applanix airborne positioning system performance specifications.

AV410 Absolute Accuracy	Post-processed
Position (m)	0.05–0.30
Velocity ( $\text{ms}^{-1}$ )	0.005
Roll and Pitch (deg)	0.008
True Heading (deg)	0.025
AV410 Relative Accuracy	
Noise ( $\text{deg h}^{-0.5}$ )	<0.1
Drift ( $\text{deg h}^{-1}$ )*	0.5

\*: attitude will drift at this rate up to the maximum absolute accuracy.

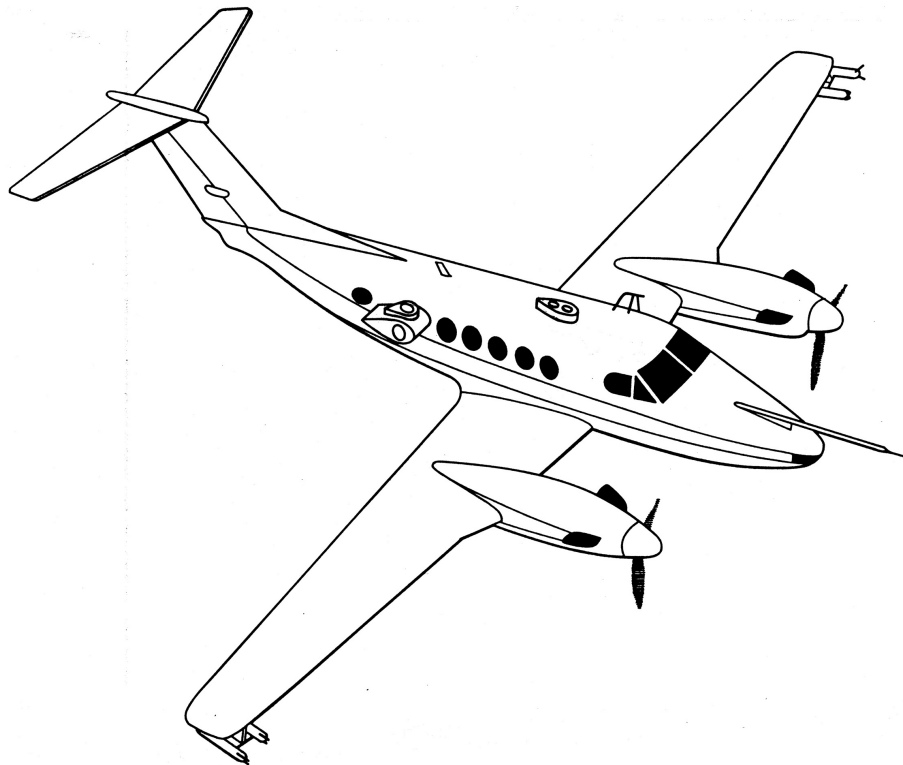


Fig. 1. UWKA showing nose boom location.

## Correction of static pressure on a research aircraft in accelerated flight

A. R. Rodi and D. C. Leon

Title Page

Abstract

Introduction

Conclusions

References

Tables

Figures



Back

Close

Full Screen / Esc

Printer-friendly Version

Interactive Discussion



## Correction of static pressure on a research aircraft in accelerated flight

A. R. Rodi and D. C. Leon

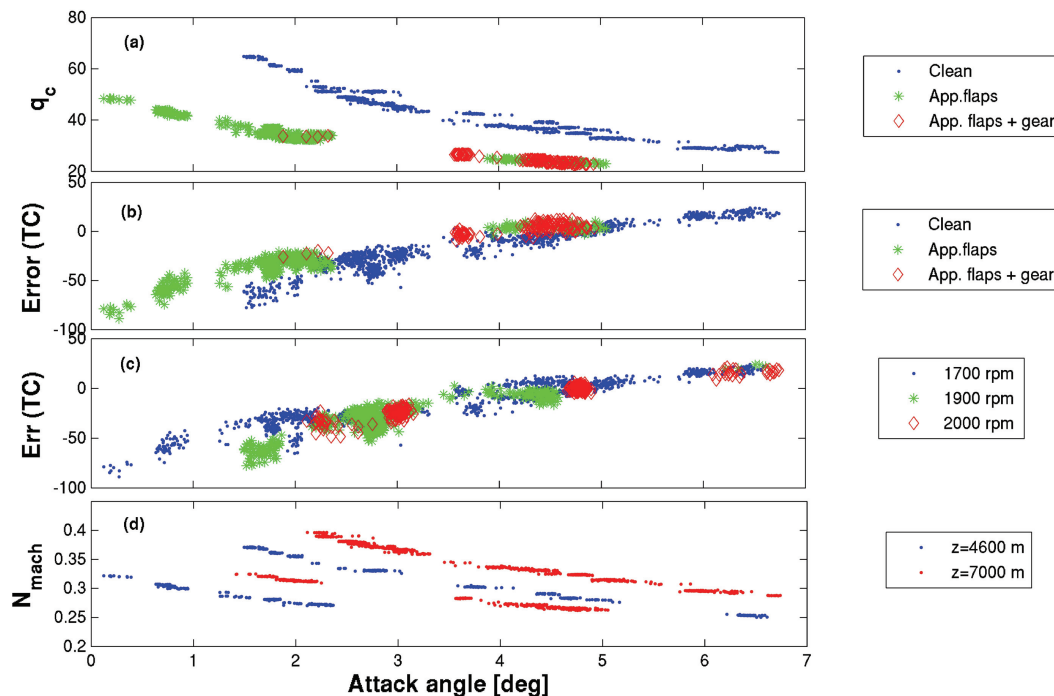


**Fig. 2.** Scatter plots (10 Hz data) as functions of attack angle [deg] for various flight configurations various and altitudes as indicated in legends: **(a)** Dynamic pressure  $q_c$  [hPa], **(b)** and **(c)** static pressure error determined by TC [hPa], and **(d)** Mach number.

Title Page

Abstract

Introduction

Conclusions

References

Tables

Figures

◀

▶

◀

▶

Back

Close

Full Screen / Esc

Printer-friendly Version

Interactive Discussion

## Correction of static pressure on a research aircraft in accelerated flight

A. R. Rodi and D. C. Leon

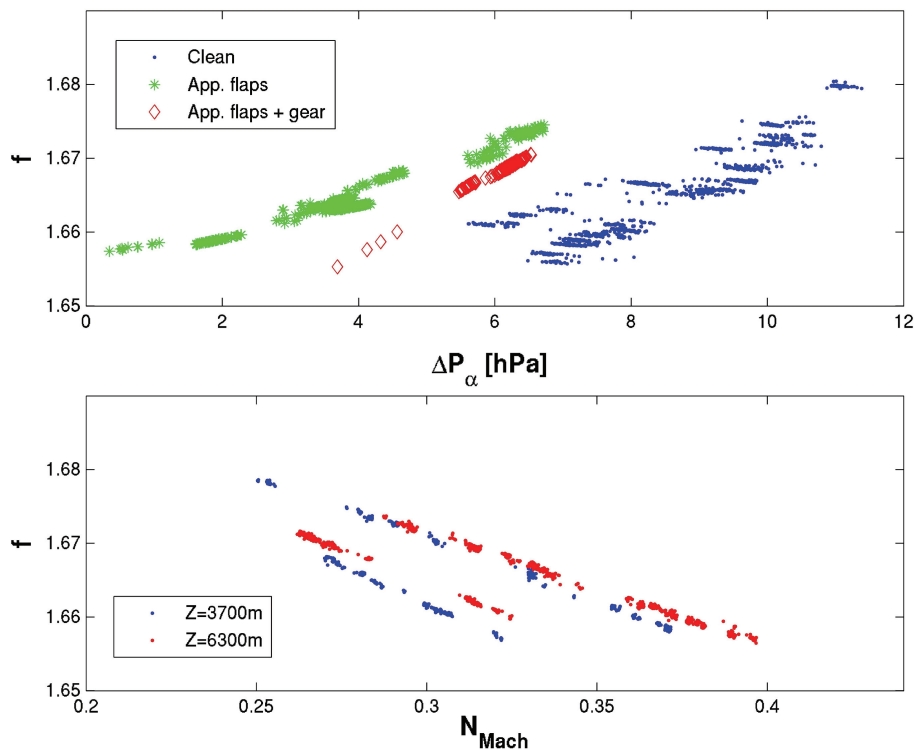


**Fig. 3.** Scatter plots (10Hz data) of probe sensitivity factor  $f$ , calculated from the solution of Eqs. (2) and (A11), versus  $\Delta P_\alpha$  [hPa] (top panel), and Mach number (bottom panel) for various flight configurations and altitudes as indicated in legend.

Title Page

Abstract

Introduction

Conclusions

References

Tables

Figures

◀

▶

◀

▶

Back

Close

Full Screen / Esc

Printer-friendly Version

Interactive Discussion

**Correction of static pressure on a research aircraft in accelerated flight**

A. R. Rodi and D. C. Leon

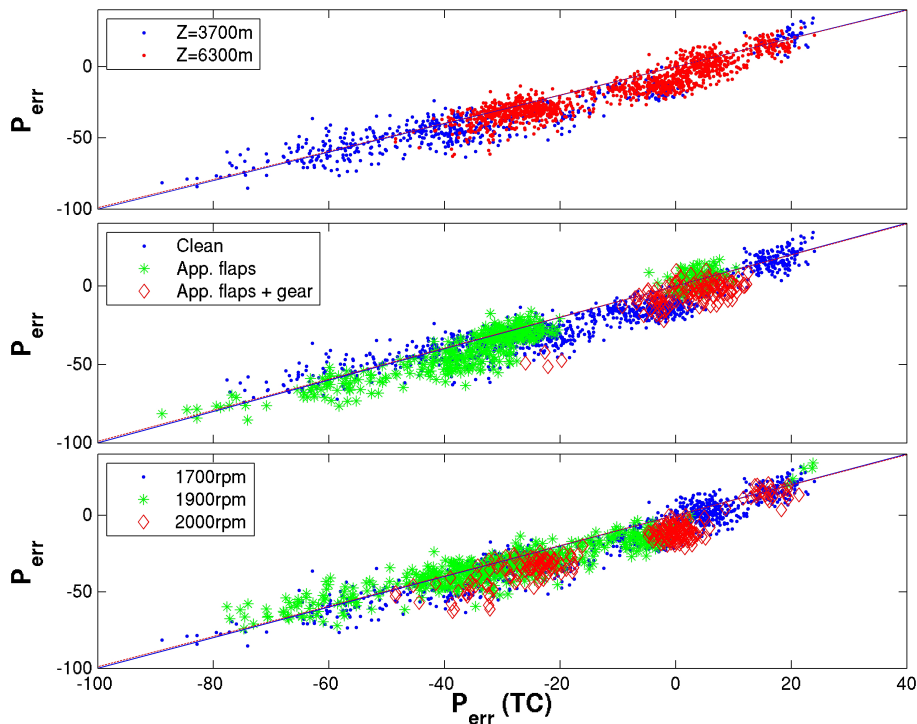


**Fig. 4.** Pressure error [Pa] predicted from differential pressure algorithm vs error measured with TC for various flight configurations, altitudes and propellor speeds as indicated in legends (10 Hz data). 1 : 1 lines are shown.

Title Page

Abstract

Introduction

Conclusions

References

Tables

Figures

◀

▶

◀

▶

Back

Close

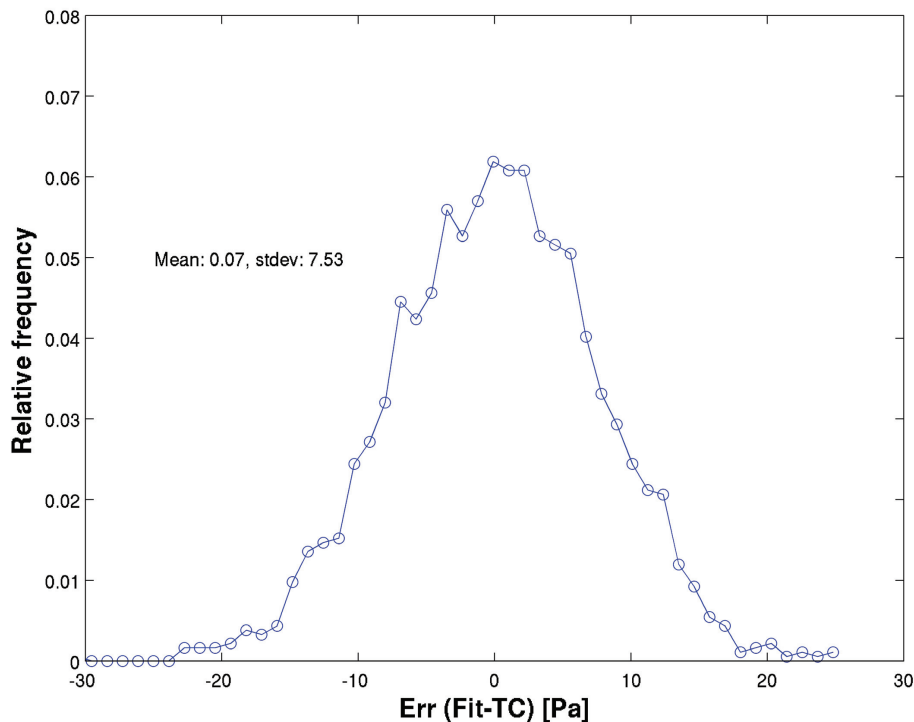
Full Screen / Esc

Printer-friendly Version

Interactive Discussion

**Correction of static pressure on a research aircraft in accelerated flight**

A. R. Rodi and D. C. Leon

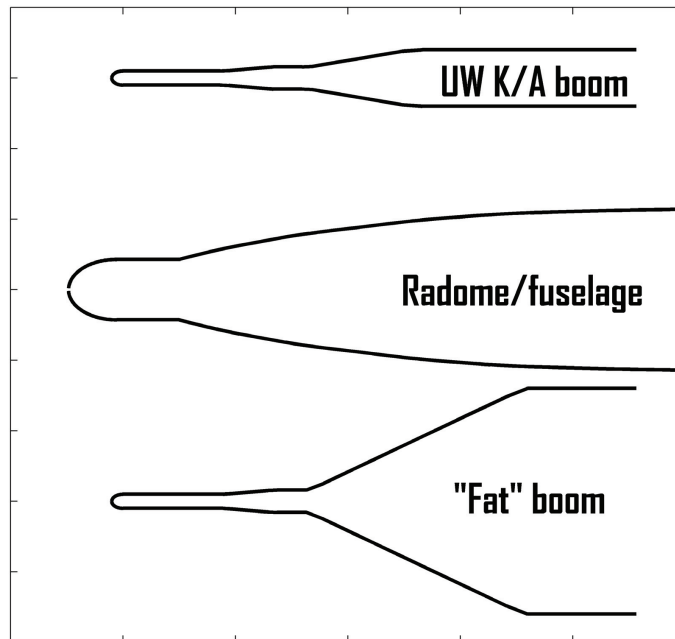


**Fig. 5.** Distribution of residual error (DP algorithm prediction minus TC measurement) [Pa] (10 Hz data).

[Title Page](#)[Abstract](#)[Introduction](#)[Conclusions](#)[References](#)[Tables](#)[Figures](#)[◀](#)[▶](#)[◀](#)[▶](#)[Back](#)[Close](#)[Full Screen / Esc](#)[Printer-friendly Version](#)[Interactive Discussion](#)

**Correction of static pressure on a research aircraft in accelerated flight**

A. R. Rodi and D. C. Leon

**Fig. 6.** Models of aircraft and boom configurations (see text).[Title Page](#)[Abstract](#)[Introduction](#)[Conclusions](#)[References](#)[Tables](#)[Figures](#)[◀](#)[▶](#)[◀](#)[▶](#)[Back](#)[Close](#)[Full Screen / Esc](#)[Printer-friendly Version](#)[Interactive Discussion](#)

**Correction of static pressure on a research aircraft in accelerated flight**

A. R. Rodi and D. C. Leon

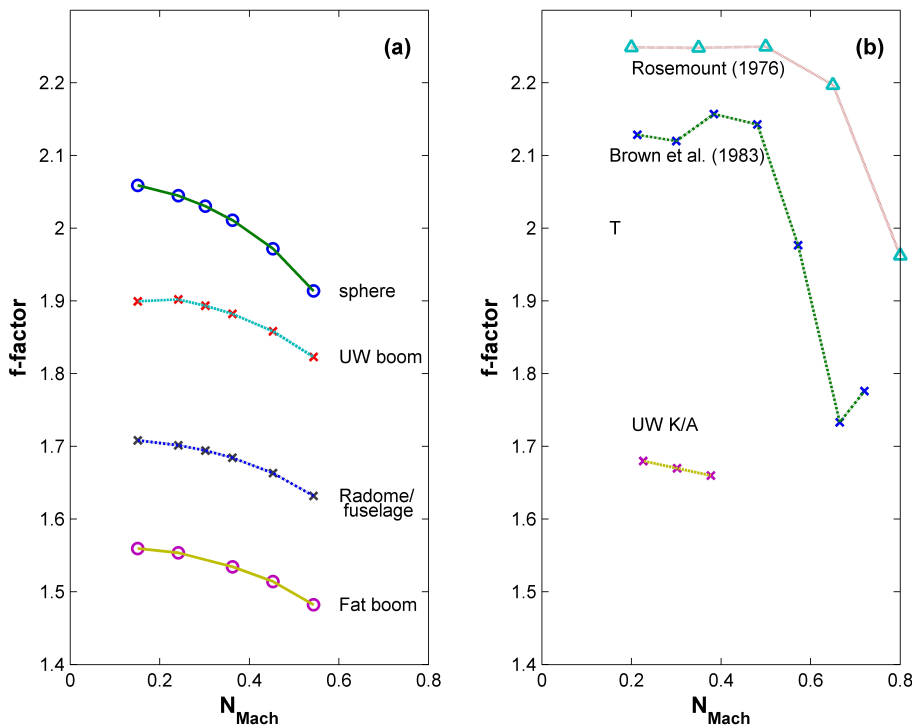


**Fig. 7.** Estimation of sensitivity factor  $f$  from (a) modeling and (b) values from Brown et al. (1983), (Rosemount, 1976), and solution to Eq. (A11) for UW King Air flight data. The point labeled “T” represents the value from determined from the wind tunnel tests of the R858 model.

Title Page

Abstract Introduction

Conclusions References

Tables Figures

◀ ▶

◀ ▶

Back Close

Full Screen / Esc

Printer-friendly Version

Interactive Discussion



**Correction of static pressure on a research aircraft in accelerated flight**

A. R. Rodi and D. C. Leon

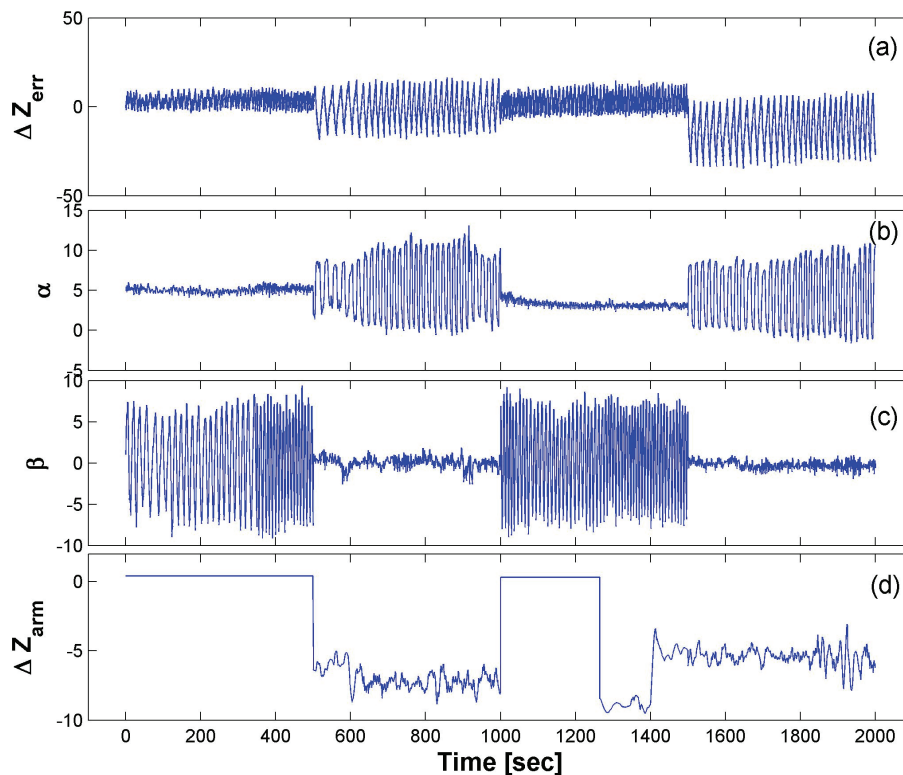


**Fig. 8.** Time series of: **(a)** Height difference (geometric-pressure) [m], **(b)** attack angle [deg], **(c)** sideslip angle [deg], and **(d)** vertical component of lever arm correction [m]. Time series is the concatenation of four 500 s segments, the first two flown at 4600 m, the second two at 7000 m.

Title Page

Abstract

Introduction

Conclusions

References

Tables

Figures

◀

▶

◀

▶

Back

Close

Full Screen / Esc

Printer-friendly Version

Interactive Discussion

---

**Correction of static pressure on a research aircraft in accelerated flight**

---

A. R. Rodi and D. C. Leon

---

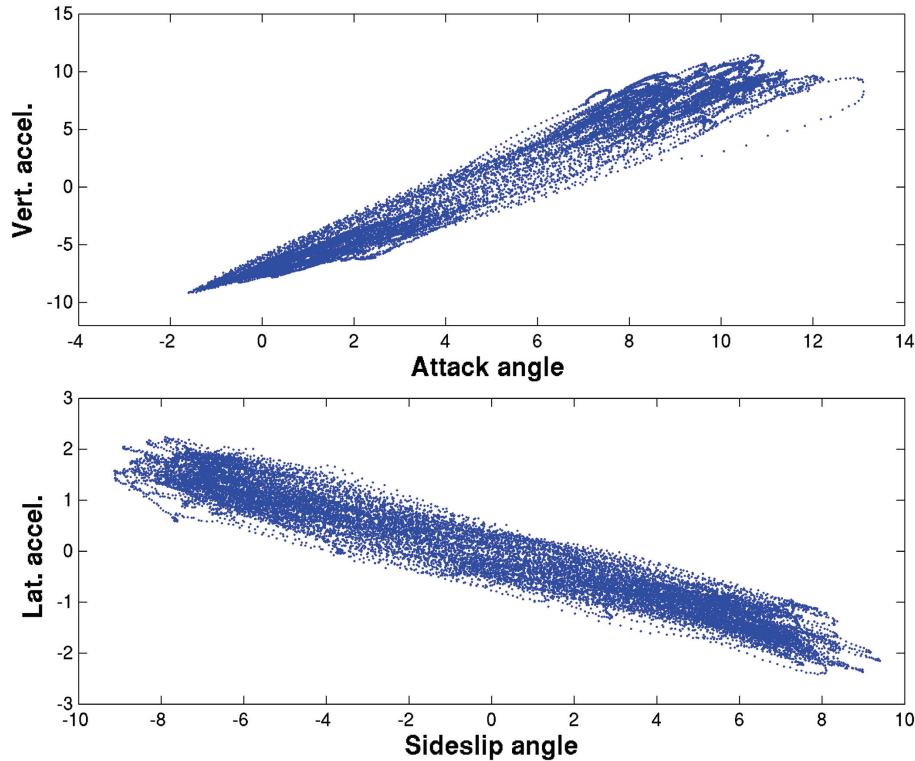


**Fig. 9.** Scatter plots of: (top panel) attack angle [deg] vs. vertical acceleration [ $\text{m s}^{-2}$ ]; and (bottom panel) sideslip angle [deg] vs. lateral acceleration [ $\text{m s}^{-2}$ ].

[Title Page](#)[Abstract](#)[Introduction](#)[Conclusions](#)[References](#)[Tables](#)[Figures](#)[⏪](#)[⏩](#)[◀](#)[▶](#)[Back](#)[Close](#)[Full Screen / Esc](#)[Printer-friendly Version](#)[Interactive Discussion](#)

**Correction of static pressure on a research aircraft in accelerated flight**

A. R. Rodi and D. C. Leon

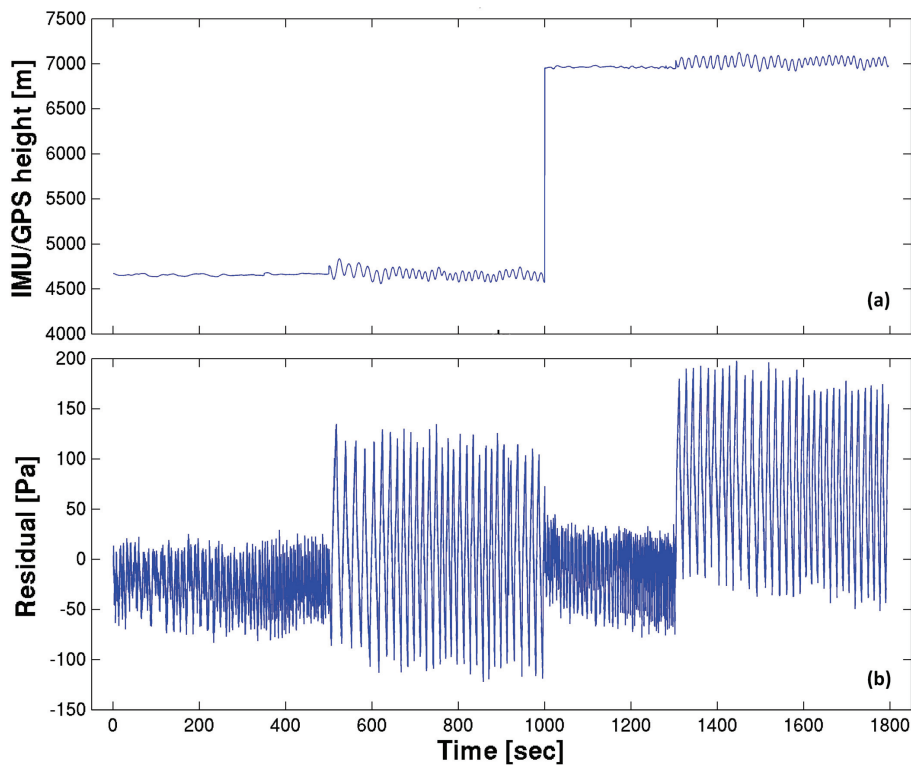


**Fig. 10.** Concatenated time series as in Fig. 8: (top panel) aircraft height [m] (m.s.l.); and (bottom panel) pressure error determined from IMU/dGPS before correction [Pa].

[Title Page](#)[Abstract](#)[Introduction](#)[Conclusions](#)[References](#)[Tables](#)[Figures](#)[◀](#)[▶](#)[◀](#)[▶](#)[Back](#)[Close](#)[Full Screen / Esc](#)[Printer-friendly Version](#)[Interactive Discussion](#)

**Correction of static pressure on a research aircraft in accelerated flight**

A. R. Rodi and D. C. Leon

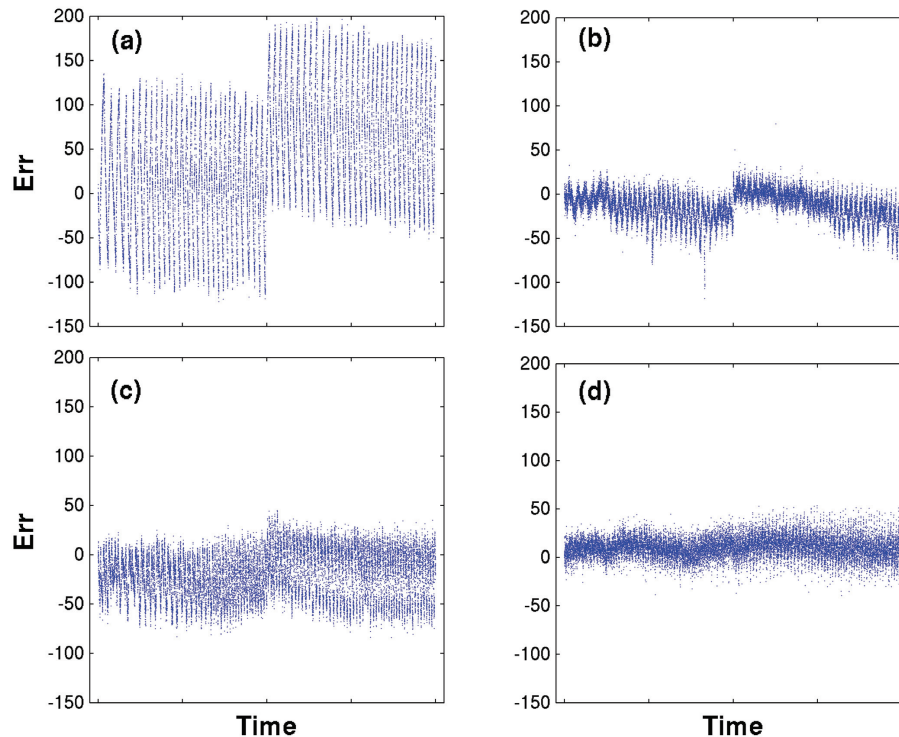


**Fig. 11.** Time series of errors [Pa] from Fig. 10: **(a)** and **(b)** are before and after correction, respectively, for attack changes; **(c)** and **(d)** before and after correction, respectively, for sideslip changes.

[Title Page](#)[Abstract](#)[Introduction](#)[Conclusions](#)[References](#)[Tables](#)[Figures](#)[◀](#)[▶](#)[◀](#)[▶](#)[Back](#)[Close](#)[Full Screen / Esc](#)[Printer-friendly Version](#)[Interactive Discussion](#)

**Correction of static pressure on a research aircraft in accelerated flight**

A. R. Rodi and D. C. Leon

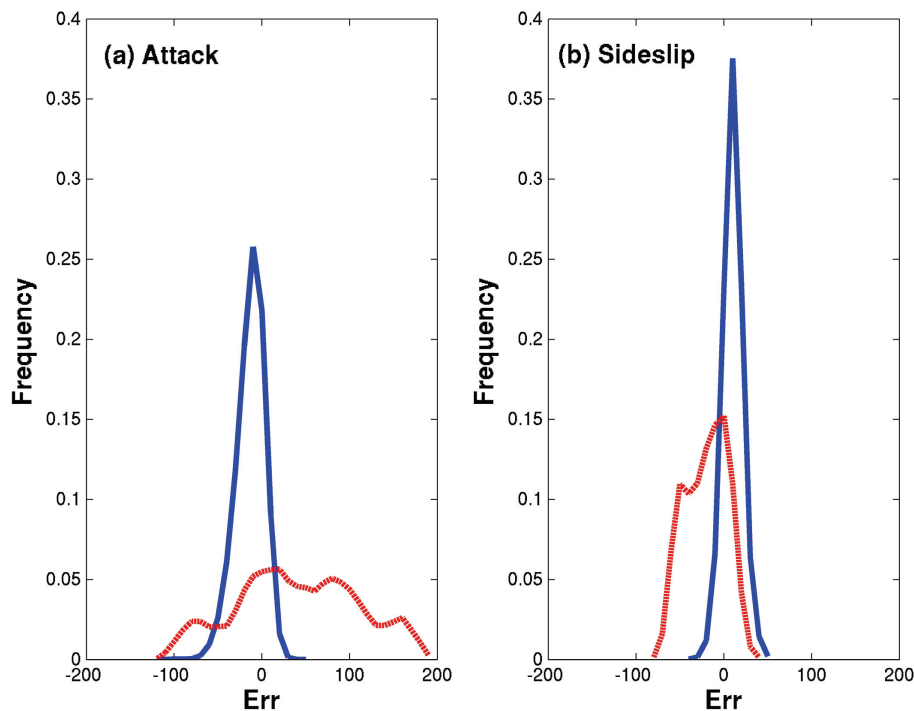


**Fig. 12.** Distribution of errors for data shown in Fig. 11 before correction (red) and residual after correction (blue) for: **(a)** Attack angle changes; and **(b)** sideslip angle changes.

[Title Page](#)[Abstract](#)[Introduction](#)[Conclusions](#)[References](#)[Tables](#)[Figures](#)[◀](#)[▶](#)[◀](#)[▶](#)[Back](#)[Close](#)[Full Screen / Esc](#)[Printer-friendly Version](#)[Interactive Discussion](#)

## Correction of static pressure on a research aircraft in accelerated flight

A. R. Rodi and D. C. Leon

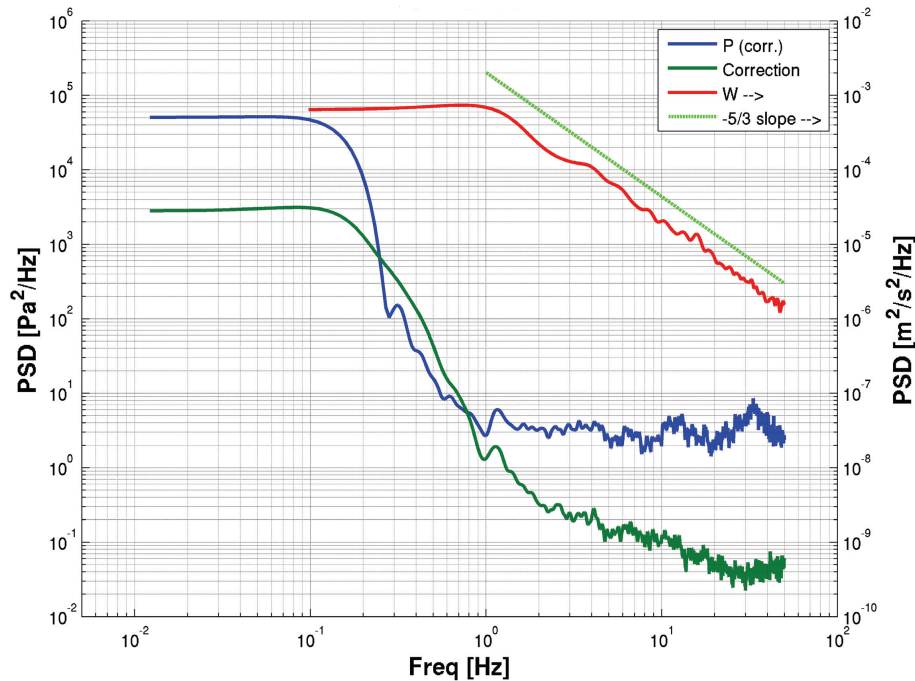


**Fig. 13.** Power spectral density [variance/frequency unit] versus frequency [Hz] for period of attack angle change at 7000 m altitude. Left axis: measured (uncorrected) static pressure [Pa], pressure correction [Pa], and corrected static pressure [Pa]. Right axis: vertical wind component [ $\text{m s}^{-1}$ ] and inertial subrange  $-5/3$  slope.

[Title Page](#)
[Abstract](#)
[Introduction](#)
[Conclusions](#)
[References](#)
[Tables](#)
[Figures](#)
[◀](#)
[▶](#)
[◀](#)
[▶](#)
[Back](#)
[Close](#)
[Full Screen / Esc](#)
[Printer-friendly Version](#)
[Interactive Discussion](#)

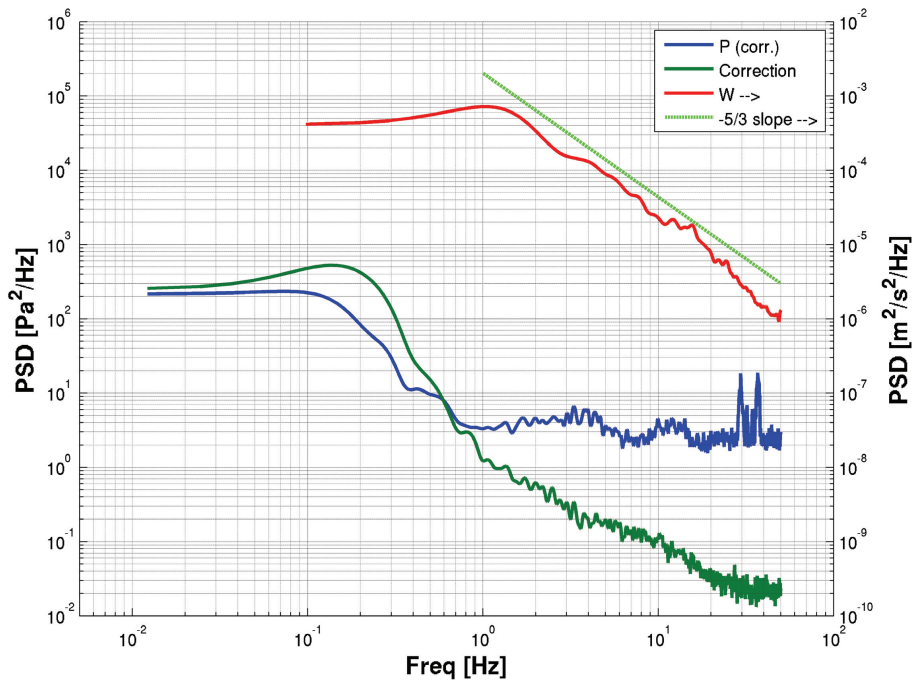


**Fig. 14.** Power spectral density as in Fig. 13 for period of sideslip angle changes at 7000 m altitude.

**Correction of static pressure on a research aircraft in accelerated flight**

A. R. Rodi and D. C. Leon

Title Page

Abstract Introduction

Conclusions References

Tables Figures

◀ ▶

◀ ▶

Back Close

Full Screen / Esc

Printer-friendly Version

Interactive Discussion

